minerals

Article

Pyrite-Hosted Inclusions in the Southern Ore Belt of the Bainaimiao Porphyry Cu Deposit: Composition and $\delta^{34}S$ Characteristics

Liwen Wu [1], Yushan Zuo [1,*], Yongwang Zhang [1], Jianjun Yang [1], Yimin Liu [1], Guobin Zhang [1], Hong Zhang [1], Peng Zhang [2] and Rui Liu [2]

[1] Inner Mongolia Key Laboratory of Magmatic Mineralization and Ore-Prospecting, Hohhot 010020, China
[2] School of Resources and Environmental Engineering, Shandong University of Technology, Zibo 255000, China

Abstract

This study presents a comprehensive case analysis of pyrite-hosted solid inclusions and their metallogenic significance in the Bainaimiao porphyry Cu deposit in NE China, which is genetically linked to the early Silurian granodiorite intrusion and porphyry dykes. Solid inclusions in pyrite from the deposit's southern ore belt were analyzed across distinct mineralization stages. Using Electron Probe Micro-Analysis (EPMA) and in situ sulfur isotope analysis (MC-ICP-MS), inclusion assemblages in pyrite were identified, including pyrrhotite-chalcopyrite solid solutions, biotite, and dolomite. The results demonstrate that these inclusions primarily formed through coprecipitation with pyrite during crystal growth. Early-stage mineralizing fluids exhibited extreme temperatures exceeding 700 °C, coupled with low oxygen fugacity (fO_2) and low sulfur fugacity (fS_2). Sulfur isotope compositions ($\delta^{34}S$: −5.85 to −4.97‰) indicate a dominant mantle-derived magmatic sulfur source, with contributions from reduced sulfur in sedimentary rocks. Combined with regional geological evolution, the Bainaimiao deposit is classified as a porphyry-type deposit. Its ore-forming materials were partially derived from Mesoproterozoic submarine volcanic exhalative sedimentary source beds, which were later modified and enriched by granodiorite porphyry magmatism.

Keywords: Bainaimiao porphyry Cu deposit; pyrite inclusions; sulfur isotopes; ore-forming fluids; porphyry-type deposit

Academic Editor: Maria Economou-Eliopoulos

Received: 12 June 2025
Revised: 9 July 2025
Accepted: 9 July 2025
Published: 12 July 2025

Citation: Wu, L.; Zuo, Y.; Zhang, Y.; Yang, J.; Liu, Y.; Zhang, G.; Zhang, H.; Zhang, P.; Liu, R. Pyrite-Hosted Inclusions in the Southern Ore Belt of the Bainaimiao Porphyry Cu Deposit: Composition and $\delta^{34}S$ Characteristics. *Minerals* **2025**, *15*, 729. https://doi.org/10.3390/min15070729

1. Introduction

As the most prevalent sulfide mineral within the Earth's crust, pyrite plays a crucial role in various hydrothermal ore systems. These systems encompass porphyry-type deposits [1], sediment- and volcanic-hosted massive sulfide (VMS) deposits [2,3], Mississippi Valley-type (MVT) deposits [4], and epithermal-type deposits [5]. Pyrite, which has genetic connections with pre-ore, syn-ore, and post-ore deposition minerals, offers distinctive perspectives on fluid evolution. Additionally, it provides valuable information regarding the physicochemical conditions (such as temperature, oxygen fugacity, and sulfur fugacity) of hydrothermal systems throughout multiple mineralization stages [6–9].

Pyrite contains numerous solid inclusions, mainly consisting of sulfides, sulfosalts, and native metals, with high concentrations of elements like Pb, Hg, Bi, Sb, Au, Ag, Ni, Te, and As [10]. These mineral inclusions are predominantly found in low-temperature

pyrite with high defect densities, and represent the principal origin of most trace elements within pyrite [10]. Hence, accurately analyzing the textures of sulfide minerals and the distributions of inclusions is essential for precisely evaluating trace-element contents and sulfur isotopes [7,8,11–13]. This analysis is especially important to prevent misestimating elemental concentrations, whether by overestimation or underestimation. In specific scenarios, the mineral inclusions hosted by pyrite can directly determine the fluid evolution processes, mechanisms of heavy-metal dissolution and transport, and pathways of ore mineral precipitation.

The objective of this research is to clarify the characteristics of solid inclusion assemblages in pyrite from the Bainaimiao porphyry copper deposit, which is located in the Central Asian Orogenic Belt, northeastern China, and is genetically related to Early Silurian granodiorite intrusions and porphyry dykes. Specifically, we aim to determine the compositions of these solid inclusions in pyrite from the southern ore belt across different mineralization stages. On this basis, we will assess the petrogenetic significance of the included mineral phases, focusing on their role in defining the ore-forming processes and the crystallization environment of the host pyrite. Furthermore, by combining microtextural observations of pyrite and associated gangue minerals, we seek to infer the physicochemical conditions (such as temperature, oxygen fugacity, and sulfur fugacity) during mineralization and establish a genetic model for the Bainaimiao copper deposit. This will help to deepen understanding of the deposit's formation mechanism and provide a scientific basis for related mineral exploration and research.

2. Geological Settings

The Bainaimiao region is located in the middle section of the accretionary orogenic belt, along the northern margin of the North China Craton (Figure 1a), with its northern boundary defined by the Ondor Sum subduction–accretionary complex belt [14] (Figure 1b). The dominant structural framework consists of NW-W-trending structures, including a series of folds, compression fracture zones, thrust faults, and schistosity zones, which control the distribution of rocks and ore deposits in this region.

The exposed strata in the area include the Middle–Late Proterozoic Bayan Obo Group, composed of slate and phyllite; the Paleozoic Baiyinduxi Group, composed of leptite and sillimanite-bearing biotite schist; the Ordovician Bainaimiao Group, composed of chlorite schist and minor sericite–feldspar–quartz schist; the Silurian Xuniwusu Formation, consisting of slate, phyllite, metasandstone, and andesitic volcanic rock; the Carboniferous Benbatu Formation, comprising graywacke, tuffaceous sandstone, and mudstone slate; the Permian Sanmianjing Formation, characterized by hard sandy and tuffaceous sandstone intercalated with limestone; and the Jurassic Daqingshan Formation, composed of acidic volcanic rock, continental facies sandy shale, and conglomerate (Figure 1c).

Magmatic activities in this area are frequent and diverse (Figure 1c), encompassing a spectrum of lithologies, from ultrabasic to acidic rocks. The intrusive rocks are predominantly Ordovician in age, including granodiorite and quartz diorite, which are distributed in the northeastern sector. In the southwestern region, Permian granite represents the dominant exposed magmatic rock unit.

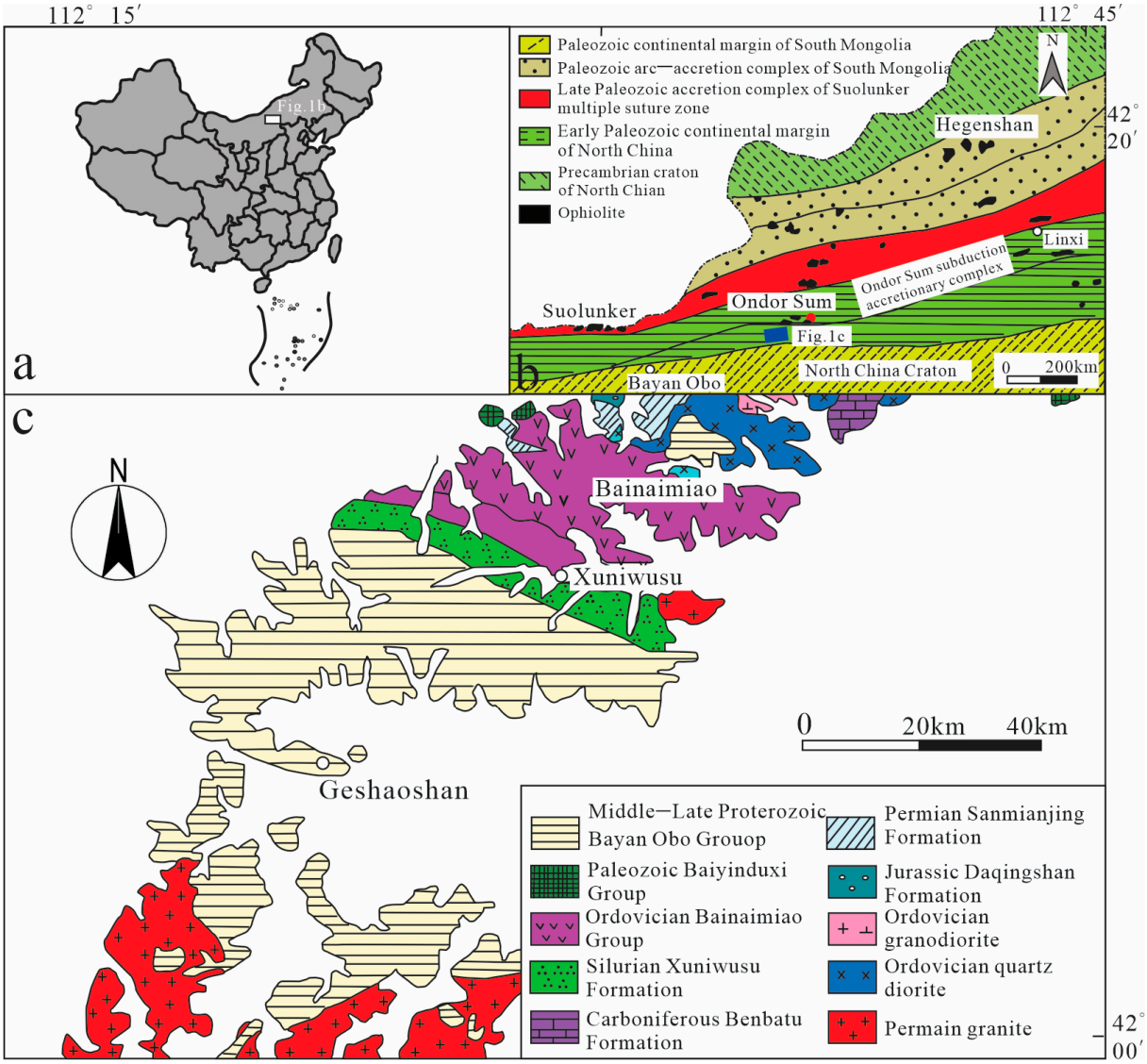

Figure 1. The location of the Bainaimiao area in China (**a**), its tectonic location (**b**) (modified from [14]), and a regional geological map (**c**) (modified from [15]) of the Bainaimiao area.

3. Ore Deposit Geology

The Bainaomiao deposit is a polymetallic deposit mainly featuring Cu, with significant associations of Au. It hosts reserves of over 0.6 million metric tons (Mt) of copper metal at an average grade of 0.8 wt.% Cu, and 20 tons (t) of Au with grades ranging from 1 to 16 g/t Au [16]. Geologically, this deposit stands out for its complex and diverse metallogenic processes, making it a key research subject for understanding the genesis and evolution of polymetallic deposits. The strata exposed within the mining area display remarkable geological diversity. The Ordovician Bainaomiao Formation provides the fundamental geological framework (Figure 2), while the Middle Silurian Xuniwusu Formation, Lower Permian Baiyinduxi Group and Sanmianjing Formation, and Upper Jurassic Daqingshan Formation each contribute unique sedimentary and tectonic features that have influenced the mineralization process. Additionally, Quaternary deposits cover the surface. The Bainaimiao Formation is the most widely distributed in the mining area. It extends nearly in an E-W direction and dips towards the S-SW. From top to bottom, it is divided into five lithologic sections. The first, third, and fifth sections are predominantly composed of greenschist; the second and fourth sections consist mainly of felsic schist, with thin interbeds

of ferruginous quartzite in select areas. Orebodies predominantly occur within the third and fifth lithologic sections of the Bainaimiao Formation. They are hosted in rock assemblages consisting of chlorite–actinolite plagioclase schist, chlorite plagioclase schist intercalated with porphyroblastic rocks, and amphibolite, as well as amphibolite interlayered with biotite plagioclase schist (illustrated in Figure 2). Silicification, sericitization, chloritization, epidotization, and carbonatization are relatively developed in the Bainaomiao deposit. In the mining region, the exposed magmatic rocks are mainly quartz diorite, granodiorite porphyry, and muscovite granite.

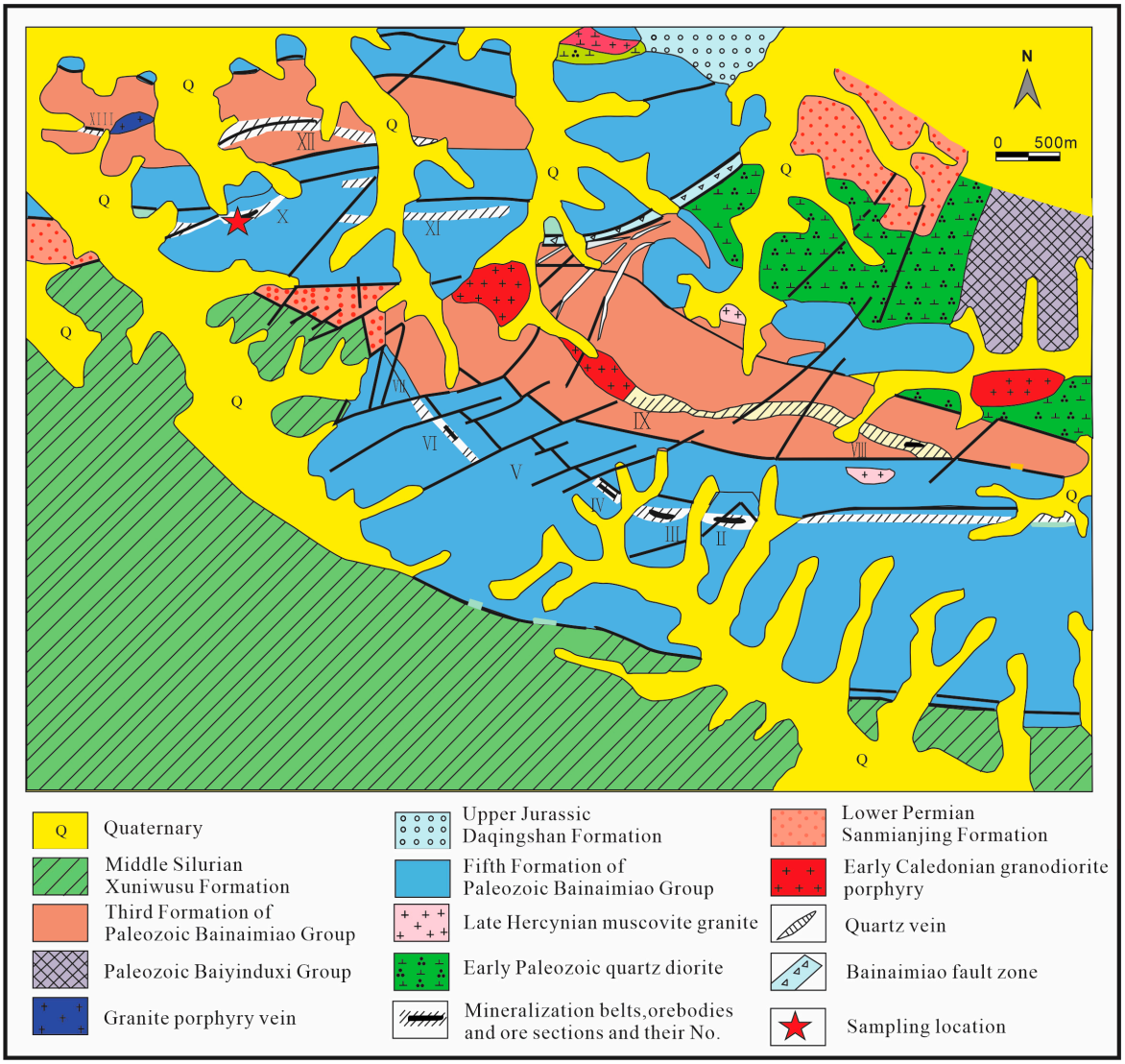

Figure 2. A geological map of the Bainaimiao Cu deposit, NE China.

Currently, twelve ore sections (labeled II–XIII) are either already in the process of exploitation or are undergoing development (refer to Figure 2). According to the spatial arrangement and geological characteristics of these sections, the deposit can be classified into two distinct belts: the southern ore belt, which encompasses ore sections II, III, IV, V, VI, VII, X, and XI; and the northern ore belt, including ore sections VIII, IX, XII, and XIII [17]. In the southern ore belt, orebodies are mainly presented in the forms of stratiform, lenticular, and vein structures, which are hosted within greenschist (as depicted in Figure 3). In the northern ore belt, the orebodies occur as fragmented bodies, predominantly hosted within the granodiorite porphyry. In the southern ore belt, the ores are predominantly

characterized by zones of sulfide dissemination with distinctive structural features, and quartz veinlets (stockwork) are less developed. Locally, fine quartz veinlets may occur, but they are not the dominant ore-bearing structure. The metallic mineral composition is mainly composed of chalcopyrite, pyrite, and molybdenite, while pyrrhotite, sphalerite, galena, bornite, cobaltite, and native gold are present in relatively smaller quantities. Gangue minerals include quartz, calcite, biotite, K-feldspar, sericite, muscovite, epidote, chlorite, and gypsum. Ore textures are characterized by granular, veinlet, disseminated, and banded mineralization (Figure 4).

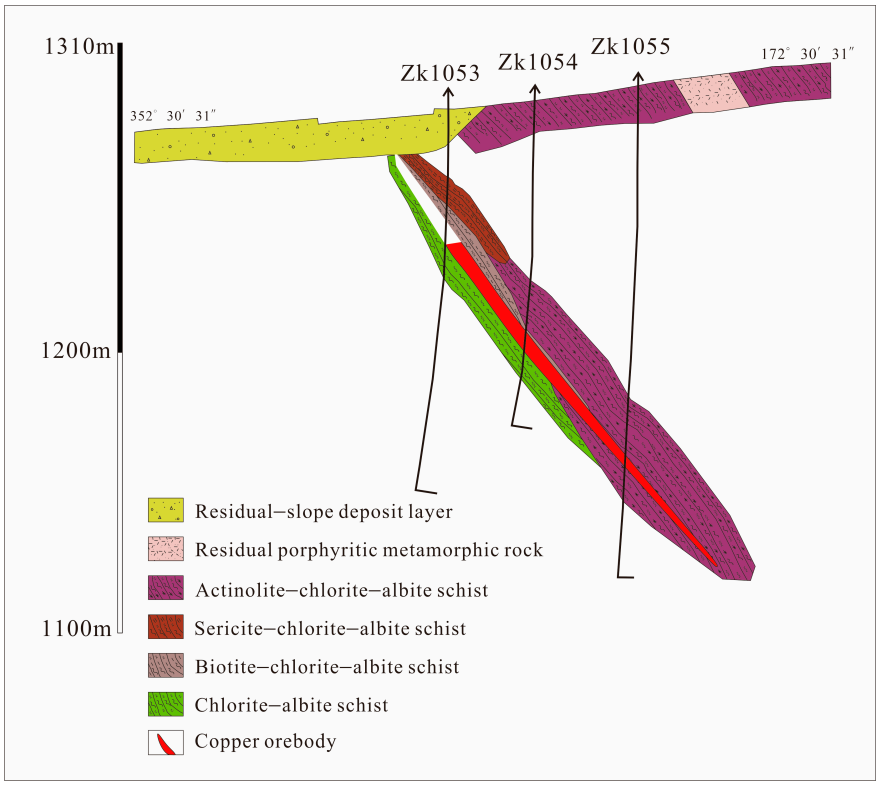

Figure 3. Exploration profile along line III in ore section X of the Bainaimiao Cu deposit, NE China.

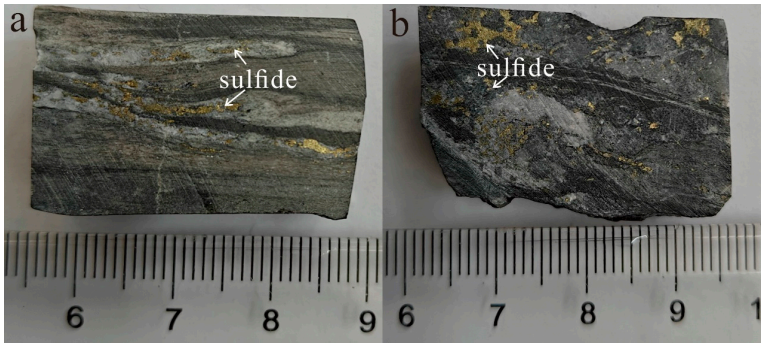

Figure 4. (**a**) Veinlet-disseminated and (**b**) mineralized greenschist in the Bainaimiao Cu deposit.

4. Sample Descriptions and Analytical Methods

The sampling locations are indicated in Figure 2. Ten ore samples were collected from the 5th Formation of the Bainaimiao Group, X ore section in the southern ore belt. The samples were derived from metamorphosed volcanic rocks (greenschists) (Figure 4). About 30 mineral inclusions were analyzed, and the typical mineral and inclusion compositions are shown in Figure 5. The samples consisted predominantly of chlorite (20%), albite (20%),

and quartz (15%), with ore minerals including pyrite, chalcopyrite, and bornite. Pyrite contained abundant inclusions.

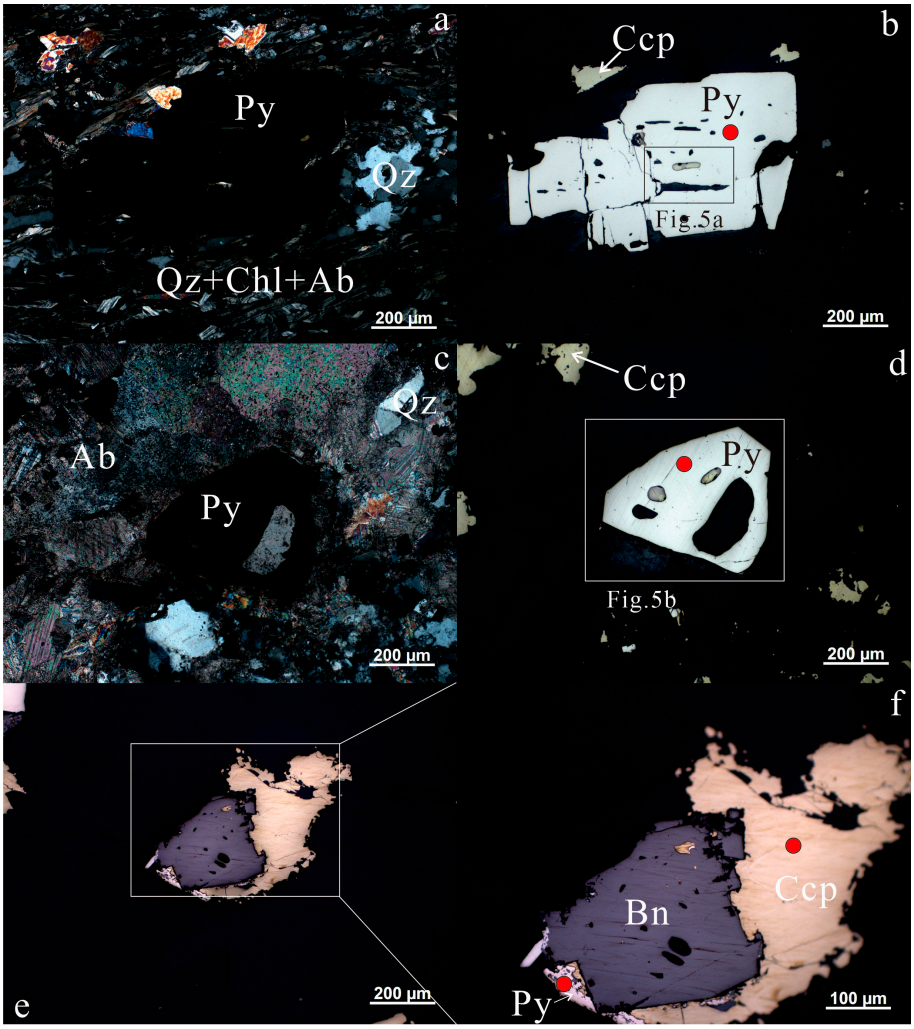

Figure 5. Microphotographs of ore minerals (**a**–**f**) in the greenschist from the Bainaimiao deposit. (**a**,**c**) are orthogonal polarized-light photographs, and (**b**,**d**,**e**,**f**) are the reflected-light photomicrographs. The red dots are the testing location of in situ sulfur isotopes. Abbreviations: Ab: albite, Chl: chlorite, Qz: quartz, Py: pyrite, Ccp: chalcopyrite, Bn: bornite.

Major- and minor-element analyses of pyrite and inclusions were conducted at the Geological Academy of Shandong Province using a JEOL JXA-8200 Superprobe electron microprobe (EPMA, Tokyo, Japan). The instrument operated with a focused beam, an acceleration voltage of 20 kV, and a beam current of 20 nA. Peak and background counting times were set as follows: 20 s and 10 s for Si, Na, Mg, Al, K, Cr, Ti, Fe, Cu, and Au; 10 s and 10 s for S, Zn, and As; and 10 s and 5 s for Pb. The detection limit was <120 μg/g for all elements.

At the Geological Academy of Shandong Province, in situ $\delta^{34}S$ analyses of pyrite, pyrrhotite, and chalcopyrite were carried out with a Thermo Fisher Neptune multi-collector inductively coupled plasma mass spectrometer (MC-ICP-MS, Thermo Fisher, Waltham, MA, USA). The analyses had a spatial resolution of approximately 10 μm (illustrated in Figures 4 and 5). The analytical conditions were strictly regulated, with the temperature maintained at 18–22 °C and the relative humidity kept below 65%. For point ablation, specific parameters were set: the diameter was typically 20–30 μm for pyrite, the energy density ranged from 3 to 5 J/cm^2, and the frequency was 5–8 Hz. During isotopic mea-

surements, ^{32}S and ^{34}S were simultaneously monitored using Faraday cups in static mode. Each measurement cycle had an integration time of 0.131 s, with 200 cycles conducted per analysis, resulting in a total acquisition time of around 27 s. Before the formal analysis, the instrumental parameters were optimized by utilizing sulfide reference materials to achieve the best performance. To reduce matrix effects, sulfide reference materials that were similar in composition to the sample matrices were selected, and a standard–sample–standard (SSS) bracketing method was adopted for mass discrimination correction.

5. Results

5.1. The Characteristics of Pyrite-Hosted Inclusions

The pyrite mostly exhibits a subhedral-to-euhedral crystal structure (Figure 5b,d). The crush structure of the pyrite is widespread (Figure 5b), but there is no sign of recrystallization of pyrite grain size. Pyrite with this kind of structure is considered to have formed in the early stage (Li et al., 2012) [16]. In addition, the most notable feature of this pyrite is its porous texture with pores and abundant mineral inclusions (Figure 6). Almost inclusions are anhedral (rounded) and up to 300 μm in size. Solid inclusions are represented by gangue phases (i.e., biotite and dolomite) and intergrowth of pyrrhotite and chalcopyrite (Table S1) proven by EMPA.

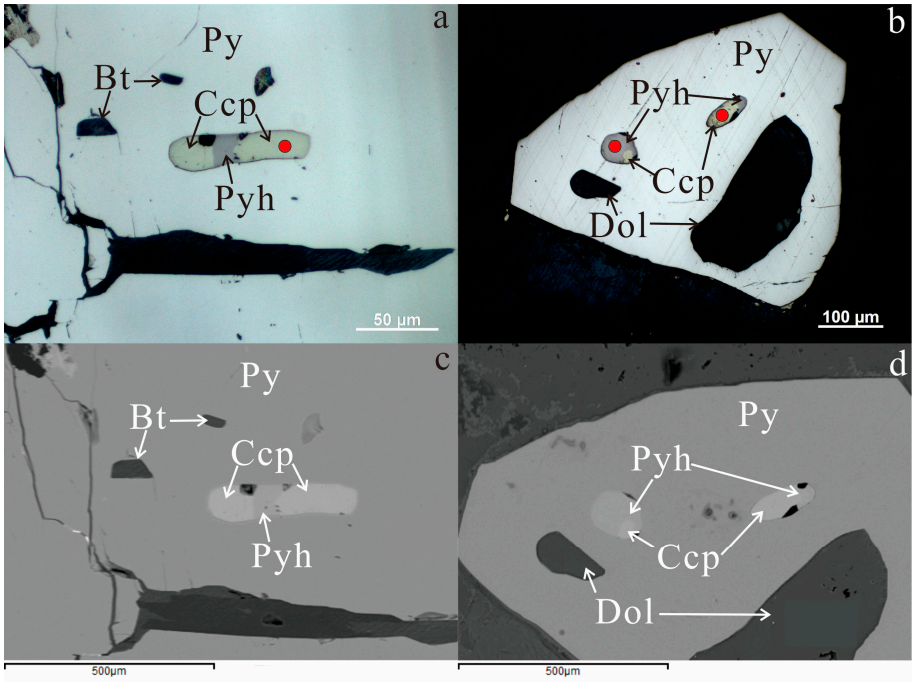

Figure 6. Reflected-light photomicrographs (**a**,**b**) of pyrite and solid inclusions, and EPMA images of pyrite and solid inclusions (**c**,**d**). The red dots are the testing location of in situ sulfur isotopes. Abbreviations: Bt: biotite, Dol: dolomite, Py: pyrite, Ccp: chalcopyrite, Pyh: pyrrhotite.

5.2. Sulfur Isotope Composition of Sulfide

In situ S isotopes in pyrite show $\delta^{34}S$ values between −5.85 to −5.63‰ (Table 1). The $\delta^{34}S$ value of bulk chalcopyrite is −5.16‰, and the $\delta^{34}S$ values of chalcopyrite in inclusions varies from −5.44 to −5.40‰. The $\delta^{34}S$ value of chalcopyrite in inclusions is −4.97‰. The $\delta^{34}S$ values of sulfide in this study have a narrow variation range, indicating that the S source of the Bainaomiao Cu deposit is relatively simple and its composition is stable. In addition, the S isotope composition of sulfides in the Bainaomiao Cu deposit is relatively close to that of mantle-derived sulfur, indicating that the S mainly comes from mantle-derived magma, but it is also mixed with reduced S from sedimentary rocks.

Table 1. Results of in situ S isotope analysis of sulfides in the Bainaimiao Cu deposit.

Mineral	$\delta^{34}S_{VCDT}$ (‰)	2σ
Pyrite in Figure 5b	−5.63	0.13
Pyrite in Figure 5d	−5.85	0.21
Pyrite in Figure 5f	−5.66	0.14
Chalcopyrite in Figure 5f	−5.44	0.29
Chalcopyrite in Figure 6a	−5.40	0.31
Chalcopyrite in Figure 6b	−5.16	0.32
Pyrrhotite in Figure 6b	−4.97	0.17

6. Discussion

6.1. The Origin of Pyrite-Hosted Inclusions

Coarse pyrite from the Bainaimiao porphyry Cu-Au deposit contains some type inclusions, comprising biotite, dolomite, pyrrhotite, and intergrowths of pyrrhotite–chalcopyrite solid solution. There are no fractures around these inclusions, which implies that the inclusions were not formed by later infilling. The origin of disseminated inclusion in pyrite possibly involves processes of exsolution [18], replacement [19], coprecipitation [20] or a mixture of the above. For the inclusions formed by exsolution, they are usually present in the form of thin lamellae within pyrite, and they are generally distributed along the crystal lattice of pyrite. In this study, inclusions mainly occur as blebs within pyrite, and there is also no relationship between the lattice orientation of the inclusions and that of pyrite. Thus, exsolution is unlikely to be the mechanism that accounts for the origin of pyrite-hosted inclusions. Furthermore, substitution is improbable as the formation mechanism for our pyrite samples. The majority of inclusions within these pyrites exist as micrometer-sized or sub-micrometer-sized blebs. Notably, there are no characteristic hydrothermal substitution textures present, such as instances where later minerals (like chalcopyrite) fill fractures within the pyrite. Consequently, it is more plausible that these inclusions formed through coprecipitation with the pyrite. This likely occurred when fluids became locally supersaturated under non-equilibrium conditions at the boundary layer of crystallizing pyrite, and were subsequently trapped by the growing pyrite crystal. As temperature and pressure decreased, daughter minerals then precipitated from the fluids entrapped within the pyrite.

6.2. Physicochemical Conditions of Early-Stage Mineralizing Fluids

Pyrite formed during the initialization stage of the Bainaimiao deposit harbors solid inclusions. These inclusions are likely to have been incidentally incorporated into the host crystals. The rapid growth rate of the pyrite crystals [21] is considered a contributing factor to this enclosure. As such, certain inclusions can serve as representative indicators. They offer valuable insights into the ore-forming processes and the associated fluid circulation patterns within the deposit.

We estimated the temperature of early-stage mineralizing fluids using the formation temperature of pyrrhotite–chalcopyrite solid solution. Experiments performed by Yund and Kullenid [22] on the S–Fe–Cu system indicated that pyrrhotite and chalcopyrite can form a solid solution at temperatures above 700 °C (Figure 7a). Thus, the temperature of early-stage mineralizing fluids is higher than 700 °C, and the pyrite probably crystallized at a high temperature (700 °C), which is consistent with the high Co/Ni ratio (Table S1). We used the mineral composition of biotite to calculate the $f(O_2)$ of the early-stage mineralizing fluids (Figure 7b). According to the temperature (>700 °C) and sulfide mineral assemblages, we estimated the sulfur fugacities of the early-stage mineralizing fluids to be low (log $f_{S2} < -2$). The oxygen fugacity is near the NNO buffer at temperatures above 700 °C according to the Fe/Fe + Mg vs. T diagram proposed by David and Hans [23], indicating

that early-stage mineralizing fluids are in reducing conditions (Figure 7c). Therefore, the early-stage mineralizing fluids have a high temperature, low oxygen fugacity, and low sulfur fugacity.

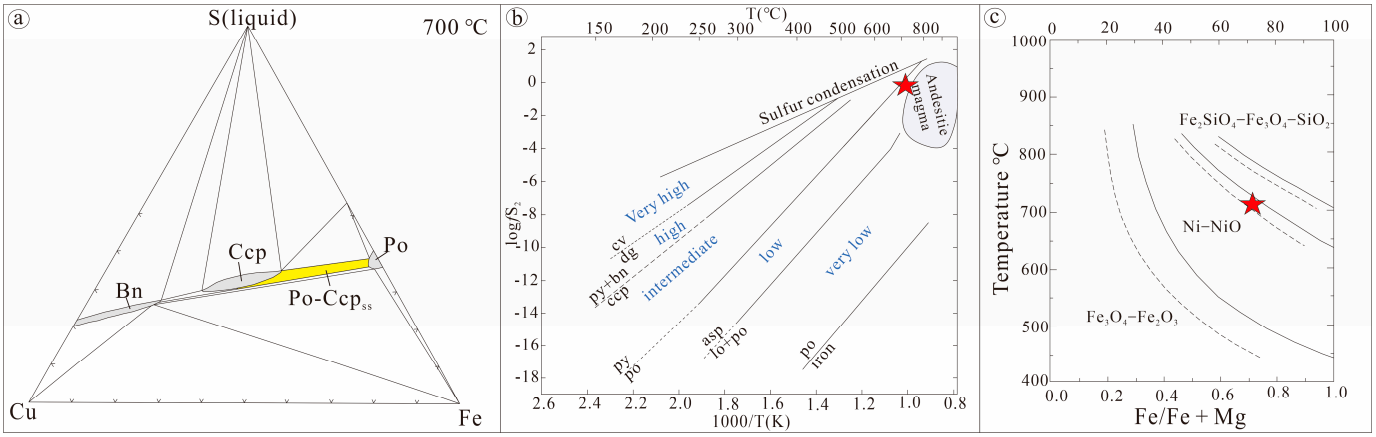

Figure 7. (**a**) A 700 °C isothermal section of the Fe−Cu−S system (modified after [22]). (**b**) A diagram of temperature vs. sulfur fugacity in the Cu−Fe−S and Fe–S systems (modified from [24]). (**c**) Fe/Fe + Mg-temperature data for biotite (modified from [23]).

6.3. The Genesis of the Bainaimiao Porphyry Cu Deposit

The genesis of the Bainaimiao deposit remains controversial, with proposed models including marine volcanic sedimentary–hydrothermal superimposition, submarine volcanic exhalative sedimentary, porphyry-type, orogenic-type, and porphyry-superimposed modification (e.g., [25–33]). This debate stems from the distinct mineralization characteristics between the southern and northern ore belts, particularly the southern belt, which preserves both porphyry-style alteration and overprinting by later orogenic processes due to complex tectono-magmatic activity which has occurred since its formation in the Late Ordovician (445 Ma; [16]). Resolving this requires focusing on early mineralization processes, as revealed by the pyrite-hosted inclusions and geochemical data from this study.

6.3.1. Key Distinctions from Alternative Genetic Models

The ore structures of submarine volcanic exhalative sedimentary ore deposits are mainly massive, banded, laminated, and brecciated, and the ore textures are mostly framboidal and colloidal, showing the fabric characteristics of chemical sedimentation. In the southern ore belts of the Bainaimiao deposit, the ores hosted in greenschist are mainly in layered, stratoid, and lenticular structures. However, areas with high ore grades have a higher content of quartz, indicating a close relationship between mineralization and silicification. The mineralization-alteration zoning of the deposit is not typical of submarine volcanic exhalative sedimentary ore deposits. Previous studies on the hydrogen and oxygen isotopes of VMS deposits have shown that the ore-forming fluid is mainly seawater, with possible admixture of magmatic water. Both the hydrogen and oxygen isotopes and the carbon and oxygen isotopes of Bainaimiao indicate that the ore-forming fluids mainly originate from the magma and mantle system [34,35]. This is inconsistent with the hydrogen and oxygen isotope characteristics of VMS deposits. Orogenic-type deposits are mainly developed in accretionary orogenic belts and collisional orogenic belts [36]. They are a kind of tectonically controlled epigenetic vein-type ore deposit occurring in metamorphic terranes, and are mainly formed in the greenschist facies environment of the middle crust. The ore-hosting strata of southern ore belts of the Bainaimiao deposit are mainly the greenschist of the Bainaimiao Formation, which has undergone medium–low-grade regional metamorphism. However, the existing precise mineralization age [16] is

earlier than the age of the occurrence of the metamorphic event [28]. This indicates that the metamorphic fluid could not be the dominant fluid for mineralization. In addition, a study of the characteristics of fluid inclusions in the Bainaimiao deposit showed that in the early and middle stages of mineralization, a large number of fluid inclusions that have medium-to-low salinity and are rich in CO_2 occur [17]. Regarding the CO_2-rich fluids, it is generally believed that there are several possible sources: mantle-derived sources, high-grade metamorphic fluids in the lower crust, and magmatic hydrothermal fluids [37–39]. Therefore, both the carbon, hydrogen, oxygen, and sulfur isotope compositions (e.g., [34,35] and this study) and fluid inclusion characteristics indicate that hydrothermal fluids from mantle and magmatic sources are the main ore-forming fluids for the Bainaimiao deposit, which differ from those of orogenic-type deposits.

6.3.2. Evidence for a Porphyry-Type Genesis of the Bainaimiao Cu Deposit

In this study, the pyrite examined was formed in the early stage of metallogenesis, and geochemical and micro-textural analysis of pyrite and pyrite-hosted inclusions can help to reveal the early-stage mineralization process. Research based on the above indicates that the temperature of early-stage mineralization fluid is higher than 700 °C, which is much higher than the ore-forming temperature of exhalative sedimentary deposits originating from hydrothermal fluid from the seafloor (metamorphic) (~200 °C), and of orogenic-type deposits (50 °C~200 °C) [40]. The hydrothermal fluid at such a high temperature should originate from magma, which is consistent with the origin of pyrite from magmatic hydrothermal fluids. In addition, pyrite usually occurs with a crush structure, also indicating that the formation of pyrite predates a tectonic metamorphic event. Therefore, we argue that the Bainaimiao deposit is a porphyry-type deposit. In addition, the inclusions of pyrrhotite–chalcopyrite solid solution indicate that some source beds existed before the formation of the early ore-forming hydrothermal fluids of the Bainaimiao deposit, which provided the ore-forming materials (e.g., S, Fe and Cu) for the subsequent ore-forming hydrothermal fluids. This is also evidenced by the in situ sulfur isotopes of sulfides. In this study, the sulfur isotopes in pyrrhotite and chalcopyrite inclusions within pyrite are almost identical to those in the host pyrite and the later chalcopyrite (Table S1). This suggests that the sulfur in both the host pyrite and the later chalcopyrite originates from the early pyrrhotite–chalcopyrite solid solution. This would seem to suggest the following generalized oxidation reaction [41]:

$$6\,(Fe_{1-X}, Cu_X)S\ \text{(pyrrhotite-chalcopyrite solid solution)} + 2(1-X)\,O_2 = 3(1-X)\,FeS_2\ \text{(pyrite)} + 6X\,CuFeS_2\ \text{(chalcopyrite)} + (1-X)\,Fe_3O_4.$$

According to the regional geological evolution process, we believe that the submarine volcanic exhalative sedimentation in the late Mesoproterozoic era formed the initial source beds containing ore-forming elements (e.g., Cu, S, and Fe). This is also confirmed by the fact that the Cu content in the intermediate-basic rocks formed during the same period is 2–3 times higher than that in similar rocks [42]. Previous studies have shown that the high initial Sr isotope ratio ($^{87}Sr/^{86}Sr$ = 0.7146, [43]) of regional Early Paleozoic granites and the low $\varepsilon Nd(t)$ values (-3.2 ± 1.7, [28]) of granodiorites also imply that Early Paleozoic magmatic rocks were formed by the mixing of juvenile crustal materials accreted from the depleted mantle and Mesoproterozoic basement [44,45]. Based on the above, it can be inferred that during the emplacement of the granodiorite porphyry in the northern ore belt of Bainaimiao, the Mesoproterozoic volcanic-sedimentary Cu-bearing source beds were heated and melted, forming S-poor and Cu-rich melts. These melts were captured by the rapidly growing pyrite. These Cu-bearing source beds also provided S and Cu for the formation of the later deposits. Due to the low oxygen fugacity of the Mesoproterozoic

Cu-bearing source beds, the sulfur isotopes of sulfides in the Bainaimiao deposit exhibit reductive characteristics. At the same time, this also endows the granodiorite porphyry in the northern ore belt of Bainaimiao with the characteristic of low oxygen fugacity, such as a low Ce^{4+}/Ce^{3+} ratio [46] and CH_4-rich fluid inclusions occurring in the early stage of metallogenesis [33].

7. Conclusions

This study conducted a comprehensive analysis of pyrite-hosted solid inclusions and their metallogenic implications in the Bainaimiao porphyry Cu deposit. The results show that pyrite from the southern ore belt contains solid inclusions such as pyrrhotite–chalcopyrite solid solutions, biotite, and dolomite, which formed through coprecipitation with pyrite during crystal growth, rather than through exsolution or replacement. In situ sulfur isotope analyses revealed $\delta^{34}S$ values ranging from −5.85 to −4.97‰, indicating a dominant mantle-derived magmatic sulfur source with minor contributions from reduced sedimentary sulfur. Geochemical and textural evidence suggests that early-stage mineralizing fluids had extreme temperatures exceeding 700 °C, coupled with low oxygen fugacity and low sulfur fugacity. Integrating these findings with regional geological data, the Bainaimiao deposit is classified as a porphyry-type deposit, where ore-forming materials were partially derived from Mesoproterozoic submarine volcanic exhalative sedimentary source beds and later modified and enriched by granodiorite porphyry magmatism. This study clarifies the origin of pyrite-hosted inclusions and quantifies key physicochemical conditions of early ore-forming fluids, providing new insights into the genetic model of this well-studied deposit.

Supplementary Materials: The following supporting information can be downloaded at https://www.mdpi.com/article/10.3390/min15070729/s1. Table S1. EMPA results of pyrite-hosted inclusions found in pyrite.

Author Contributions: Methodology, Y.Z. (Yushan Zuo); Software, Y.Z. (Yongwang Zhang) and P.Z.; Formal analysis, Y.L.; Resources, J.Y. and H.Z.; Data curation, G.Z.; Writing—original draft, L.W.; Writing—review & editing, R.L. All authors have read and agreed to the published version of the manuscript.

Funding: This research was funded by [National Natural Science Foundation of China] grant number [42102076], [Shandong Provincial Natural Science Foundation] grant number [ZR2021QD037], and [Natural Science Foundation of Inner Mongolia Autonomous Region of China] grant number [2024MS04027 and 2025MS04018].

Data Availability Statement: The original contributions presented in this study are included in the article/Supplementary Materials. Further inquiries can be directed to the corresponding authors.

Acknowledgments: We would like to thank Ma Shaoting from Shandong Academy of Geological Sciences for her assistance in the testing of this research.

Conflicts of Interest: The authors declare no conflict of interest.

References

1. Reich, M.; Deditius, A.; Chryssoulis, S.; Li, J.W.; Ma, C.Q.; Parada, M.A.; Barra, F.; Mittermayr, F. Pyrite as a record of hydrothermal fluid evolution in a porphyry copper system: A SIMS/EMPA trace element study. *Geochim. Cosmochim. Acta* **2013**, *104*, 42–62. [CrossRef]
2. Huston, D.L.; Sie, S.H.; Suter, G.F.; Cooke, D.R.; Both, R.A. Trace elements in sulfide minerals from eastern Australian volcanic-hosted massive sulfide deposits: Part I. Proton microprobe analyses of pyrite, chalcopyrite, and sphalerite, and part II. Selenium levels in pyrite: Comparison with δ34S values and impli. *Econ. Geol.* **1995**, *90*, 1167–1196. [CrossRef]
3. Basori, M.B.I.; Gilbert, S.; Large, R.R.; Zaw, K. Textures and trace element composition of pyrite from the Bukit Botol volcanic-hosted massive sulphide deposit, Peninsular Malaysia. *J. Asian Earth Sci.* **2018**, *158*, 173–185. [CrossRef]

4. Leach, D.L.; Taylor, R.D.; Fey, D.L.; Diehl, S.F.; Saltus, R.W. A deposit model for Mississippi Valley-type lead-zinc ores. In *Chapter A of Mineral Deposit Models for Resource Assessment*; USGS: Reston, VA, USA, 2010; Volume 107.
5. Shikazono, N. Precipitation mechanisms of barite in sulfate-sulfide deposits in back-arc basins. *Geochim. Cosmochim.* **1994**, *58*, 2203–2213. [CrossRef]
6. Lindaas, S.E.; Kulis, J.; Campbell, A.R. Near-infrared observation and microthermometry of pyrite-hosted fluid inclusions. *Econ. Geol.* **2002**, *97*, 603–618. [CrossRef]
7. Large, R.R.; Maslennikov, V.V.; Robert, F.; Danyushevsky, L.V.; Chang, Z. Multistage sedimentary and metamorphic origin of pyrite and gold in the Giant Sukhoi log deposit, Lena Gold Province, Russia. *Econ. Geol.* **2007**, *102*, 1233–1267. [CrossRef]
8. Large, R.R.; Danyushevsky, L.; Hollit, C.; Maslennikov, V.; Meffre, S.; Gilbert, S.; Bull, S.; Scott, R.; Emsbo, P.; Thomas, H.; et al. Gold and Trace Element Zonation in Pyrite Using a Laser Imaging Technique: Implications for the Timing of Gold in Orogenic and Carlin-style Sediment-Hosted Deposits. *Econ. Geol.* **2009**, *104*, 635–668. [CrossRef]
9. Dmitrijeva, M.; Cook, N.J.; Ehrig, K.; Ciobanu, C.L.; Metcalfe, A.V.; Kamenetsky, M.; Kamenetsky, V.S.; Gilbert, S. Multivariate statistical analysis of trace elements in pyrite: Prediction, bias and artefacts in defining mineral signatures. *Minerals* **2020**, *10*, 61. [CrossRef]
10. Deditius, A.P.; Utsunomiya, S.; Reich, M.; Kesler, S.E.; Ewing, R.C.; Hough, R.; Walshe, J. Trace metal nanoparticles in pyrite. *Ore Geol. Rev.* **2011**, *42*, 32–46. [CrossRef]
11. Cook, N.J.; Ciobanu, C.L.; Mao, J. Textural control on gold distribution in As-free pyrite from the Dongping, Huangtuliang and Hougou gold deposits, North China Craton (Hebei Province, China). *Chem. Geol.* **2009**, *264*, 101–121. [CrossRef]
12. Cook, N.J.; Ciobanu, C.L.; Meria, D.; Silcock, D.; Wade, B. Arsenopyrite-pyrite association in an orogenic gold ore: Tracing mineralization history from textures and trace elements. *Econ. Geol.* **2013**, *108*, 1273–1283. [CrossRef]
13. Voute, F.; Hagemann, S.G.; Evans, N.J.; Villanes, C. Sulfur isotopes, trace element, and textural analyses of pyrite, arsenopyrite and base metal sulfides associated with gold mineralization in the Pataz-Parcoy district, Peru: Implication for paragenesis, fluid source, and gold deposition mechanisms. *Miner. Depos.* **2019**, *54*, 1077–1100. [CrossRef]
14. Xiao, W.J.; Windley, B.F.; Hao, J.; Zhai, M. Accretion leading to collision and the Permian Solonker suture, Inner Mongilia, China: Termination of the Central Asian Orogenic Belt. *Tectonics* **2003**, *22*, 1069. [CrossRef]
15. Liu, C.F.; Liu, W.C.; Wang, H.P.; Zhou, Z.G.; Zhang, H.F.; Tang, Y.J. Geochronology and geochemistry of the Bainaimiao metavolcanic rocks in the Northern margin of North China Craton. *Acta Geol. Sin.* **2014**, *88*, 1273–1287.
16. Li, W.; Hu, C.; Zhong, R.; Xu, C.; Zhu, F. U–Pb, Ar^{39}/Ar^{40} geochronology of the metamorphosed volcanic of the Bainaimiao Group in the central Inner Mongolia and its implications for ore genesis and geodynamic setting. *J. Asian Earth Sci.* **2012**, *97*, 251–259. [CrossRef]
17. Li, J.W.; Zhao, S.B.; Huang, G.J.; Ma, R. Origin of Bainaimiao copper deposit, Inner Mongolia. *Geol. Prospect.* **2007**, *43*, 1–5.
18. Shimazaki, H. Cooling history of orebody recorded in sphalerite: An example from the Tsumo skarn deposits, Japan. *J. Fac. Sci. Univ. Tokyo Sect. II* **1980**, *20*, 61–76.
19. Govindarao, B.; Pruseth, K.L.; Mishra, B. Sulfide partial melting and chalcopyrite disease: An experimental study. *Am. Mineral.* **2018**, *103*, 1200–1207. [CrossRef]
20. Bortnikov, N.S.; Genkin, A.D.; Dobrovol'Skaya, M.G.; Muravitskaya, G.N.; Filimonova, A.A. The nature of chalcopyrite inclusions in sphalerite; exsolution, coprecipitation, or "disease"? *Econ. Geol.* **1991**, *86*, 1070–1082. [CrossRef]
21. Naglik, B.; Dumańska-Słowik, M.; Toboła, T.; Derkowski, P.; Habryn, R.; Markowiak, M. Diversity of Pyrite-Hosted Solid Inclusions and Their Metallogenic Implications—A Case Study from the Myszków Mo–Cu–W Porphyry Deposit (the Kraków–Lubliniec Fault Zone, Poland). *Minerals* **2021**, *11*, 1426. [CrossRef]
22. Yund, R.A.; Kullerud, G. Thermal stability of assemblages in the Cu—Fe—S system. *J. Petrol.* **1966**, *7*, 454–488. [CrossRef]
23. David, R.W.; Hans, P.E. Stability of biotite: Experiment, theory, and application. *Am. Mineral. J. Earth Planet. Mater.* **1965**, *50*, 1228–1272.
24. Lusk, J.; Bray, D.M. Phase relations and the electrochemical determination of sulfur fugacity for selected reactions in the Cu–Fe–S and Fe–S systems at 1 bar and temperatures between 185 and 460 C. *Chem. Geol.* **2002**, *192*, 227–248. [CrossRef]
25. Feng, X.X.; Yao, S.Z.; Duan, M.; Wang, J.Y.; Qu, K.; Wei, J.L.; Li, G.Y.; Zhu, Q. LA-ICP-MS zircon U-Pb dating of the gold-bearing quartz veins in the Bainaimiao Au deposit of Inner Mongolia and its geological significance. *Geol. Bull. China* **2014**, *33*, 1492–1501.
26. Wang, J.P.; Liu, J.J.; Jiang, X.D.; Wang, B.; Jiang, S.M. Ar-Ar dating of biotite from the Haoyao'erhudong Au deposit, Inner Mongolia and its geological significance. *Acta Mineral. Sin.* **2011**, *S1*, 643–644.
27. Zhao, Y.; Wang, J.P.; Yang, Z.H.; Liao, D.J.; Lian, C.Y.; Liu, C.H.; Li, C.F.; Xue, Y.S.; Zuo, H.Y.; Yang, G. Stable Isotopic Geochemistry of the Bainaimiao Copper Deposit. *Acta Geol. Sin. Engl. Ed.* **2014**, *88*, 660–661. [CrossRef]
28. Nie, F.J.; Pei, R.F.; Wu, L.S.; Zhang, H.T. *Magmatic Activity and Metallogeny of the Bainaimiao District, Inner Mongolia, People's Republic of China*; Beijing Science and Technology Press: Beijing, China, 1993; pp. 121–145.

29. Li, W.; Zhong, R.; Xu, C.; Song, B.; Qu, W. U–Pb and Re–Os geochronology of the Bainaimiao Cu–Mo–Au deposit, on the northern margin of the North China Craton, Central Asia Orogenic Belt: Implications for ore genesis and geodynamic setting. *Ore Geol. Rev.* **2012**, *48*, 139–150. [CrossRef]
30. Mao, J.W.; Zhou, Z.H.; Wu, G.; Jiang, S.H.; Liu, C.L.; Li, H.M.; Ouyang, H.G.; Liu, J. Metallogenic regularity and minerogenetic series of ore deposits in Inner Mongolia and adjacent areas. *Min. Depos.* **2013**, *32*, 715–729.
31. Li, W.B.; Chen, Y.J.; Lai, Y.; Ji, J.Q. Metallogenic time and tectonic setting of the Bainaimiao Cu-Au deposit, Inner Mongolia. *Acta Petrol. Sin.* **2008**, *24*, 890–898.
32. Xin, H.B. Geological Characteristics and Genesis of the Bainaimiao Copper-Polymetallic Deposit, Inner Mongolia. *Contrib. Geol. Miner. Resour.* **2006**, *4*, 236–240+298.
33. Zhou, Z.H.; Mao, J.W.; Ma, X.H.; Che, H.W.; Ou'yang, H.G.; Gao, X. Geochronological framework of the early Paleozoic Bainaimiao Cu-Mo-Au deposit, NE China, and its tectonic implications. *J. Asian Earth Sci.* **2017**, *144*, 323–338. [CrossRef]
34. Zhao, Y. *Geological and Geochemical Characteristics of the Bainaimiao Copper Deposit in Inner Mongolia and Its Geological Significance*; China University of Geosciences Beijing: Beijing, China, 2013.
35. Feng, X.X.; Yao, S.Z.; Duan, M.; Qu, K.; Wang, J.Y.; Feng, X.B.; Li, C.; Zhou, L.M. Re-Os dating of molybdenite from the Bainaimiao Cu (Mo) deposit in Inner Mongolia and its geological significance. *J. Jilin Univ. Earth Sci. Ed.* **2015**, *45*, 132–141.
36. Chen, Y.J.; Ni, P.; Fan, H.R.; Pirajno, F.; Lai, Y.; Su, W.C.; Zhang, H. Diagnostic fluid inclusions of different types hydrothermal gold deposits. *Acta Petrol. Sin.* **2007**, *9*, 2085–2108.
37. Rosenbaum, J.M.; Zindler, A.; Rubenstone, J.L. Mantle fluids: Evidence from fluid inclusions. *Geochim. Cosmochim. Acta* **1996**, *60*, 3229–3252. [CrossRef]
38. Diamond, L.W. Review of the systematics of CO_2–H_2O fluid inclusions. *Lithos* **2001**, *55*, 69–99. [CrossRef]
39. Wilkinson, J.J. Fluid inclusions in hydrothermal ore deposits. *Lithos* **2001**, *55*, 229–272. [CrossRef]
40. Chen, Y.J. Orogenic-type deposits and their metallogenic model and exploration potential. *Geol. China* **2006**, *33*, 1181–1196.
41. Harlov, D.E. Apparent pyrrhotite-chalcopyrite solid solutions in charnockites: The Shevaroy Hills Massif, Tamil Nadu, S India and the Bamble Sector, SE Norway. *Mineral. Mag.* **2000**, *64*, 853–865. [CrossRef]
42. Han, J. *Study on Geological Characteristics and Metallogenic Regularity of the Bainaimiao Copper Deposit, Siziwang Banner, Inner Mongolia Autonomous Region*; 103 Geological Brigade Printing House: Ulanqab, China, 1987; pp. 1–105.
43. Ji'an, S. Continental crust accretion and tectono-magmatic activity at the northern margin of the Sino-Korean plate. *J. Southeast Asian Earth Sci.* **1989**, *3*, 57–62. [CrossRef]
44. Wu, J.H.; Li, H.; Xi, X.S.; Kong, H.; Wu, Q.H.; Peng, N.L.; Wu, X.M.; Cao, J.Y.; Gabo-Ratio, J.A.S. Geochemistry and geochronology of the mafic dikes in the Taipusi area, northern margin of North China Craton: Implications for Silurian tectonic evolution of the Central Asian Orogen. *J. Earth Syst. Sci.* **2017**, *126*, 64. [CrossRef]
45. Zhou, Z.G.; Zhang, D.; Gu, Y.C.; Wang, G.S.; Li, H.Y.; Yu, Y.S.; Liu, C.F.; Liu, W.C. Characteristics of Bainaimiao thrust belt along Central Inner Mongolia in North China and its geological significance. *Geotecton. Metallog.* **2018**, *42*, 1–17.
46. Ma, G.; Shen, P.; Pan, H.D.; Chao, C.; Feng, H.X.; Zhou, M.H. Zircon U-Pb geochronology, trace element composition and geochemistry of ore-bearing porphyry in Bainaimiao Cu-Au deposit, Inner Mongolia, and the implications for mineralization. *Acta Geol. Sin.* **2019**, *93*, 3144–3165.